Applied Catalysis B: Environmental 325 (2023) 122330

Contents lists available at ScienceDirect

Applied Catalysis B: Environmental

journal homepage: www.elsevier.com/locate/apcatb

Synthesis of high-grade Jet fuel blending precursors by aldol condensation of lignocellulosic ketones using HfTPA/MCM-41 with strong acids and enhanced stability

Qi Li [a], Genkuo Nie [a,*], Hongyu Wang [b], Ji-Jun Zou [c,g], Shitao Yu [a], Hailong Yu [a], Xin Jin [d], Dongpei Zhang [d], Huibing Shi [e,f], Deming Zhao [e,f]

[a] Key Laboratory of Multiphase Flow Reaction and Separation Engineering of Shandong Province, College of Chemical Engineering, Qingdao University of Science and Technology, 53 Zhengzhou Road, Qingdao 266042, China
[b] State Key Laboratory of Safety and Control for Chemicals, SINOPEC Research Institute of Safety Engineering, Qingdao 266071, China
[c] Key Laboratory for Green Chemical Technology of the Ministry of Education, School of Chemical Engineering and Technology, Tianjin University, Tianjin 300072, China
[d] State Key Laboratory of Heavy Oil Processing, China University of Petroleum, Qingdao 266580 China
[e] Shandong Chambroad Petrochemicals Co., Ltd., Binzhou 256500, China
[f] Shandong Provincial Key Laboratory of Olefin Catalysis and Polymerization, Ltd., Binzhou 256500, China
[g] Collaborative Innovative Center of Chemical Science and Engineering (Tianjin), Tianjin 300072, China

ARTICLE INFO

Keywords:
Lignocellulosic ketones
Aldol condensation
Solid acid catalyst
Jet fuel precursors

ABSTRACT

Upgrading lignocellulosic ketones to Jet fuel precursors by aldol condensation is the key step for the synthesis of high-grade bio-Jet fuels. State-of-art works are confined in pure feedstock used, catalysis sites leaching and coking. Therefore, we synthesized a strong solid acid HfTPA/MCM-41 and used it to catalyze aldol condensation of lignocellulosic ketone mixture to bio-jet fuel blending precursors, where 80 %$Hf_{1.5}$TPA/MCM-41 shows better activity than 80 %HPW/MCM-41 and commercial zeolites with 66.8 % yield of products obtained. The good performance of the catalyst is ascribed to good acid properties, large surface area and especially new strong L acids and good stability based on anti-coking and water tolerance by Hf doping, which changes the electronic structure of the catalyst surface to efficiently activate C═O bond of ketones to form a metal enolate intermediate and anchoring HPW from leaching. This work demonstrates an efficient way to synthesize high-performance acid catalyst applied in bio-jet fuel synthesis.

1. Introduction

With the concern for sustainable development and fulfilling the carbon peaking and carbon neutrality goals, it is promising to develop new energy using biomass to substitute fossil ones. Bio-jet fuels are special type of aviation oil with polycyclic hydrocarbons as base component synthesized using biomass and this type of aviation oil is usually used in the volume limited aircrafts like missile and rocket [1]. In general, it needs two steps to synthesize bio-jet fuels, that is the structure of multi-ring fuel precursors and following with the hydrogenation of precursors [1], where the carbon skeleton structure of precursors plays a decisive role for the properties of synthetic fuel molecules. However, it is still a challenge to synthesize pure fuel with high performance, such as high density (0.780–1.080 g/mL) and good low-temperature properties (low freezing point < -47 °C) and low viscosity) (ASTM D1655–18, MIL-DTL-87107E, MIL-DTL-38219D). In order to obtain a good bio-jet fuel, it is a good method to develop fuel blending by combining the advantages of different fuel compositions [2]. Of course, the key step of this method is the synthesis of mixture precursors of Jet fuel blending.

Along with the development of lignocellulose conversion to furan aldehydes, aldol condensation has been commonly used for the synthesis of bio-jet fuel precursors. Cyclopentanone and cyclohexanone are selective hydrogenation products of furfural and phenol respectively, both of which have been produced industrially using agriculture wastes and forest residues [3,4]. Meanwhile, cyclic ketones, furan aldehyde and phenols are main compositions of bio-oil produced by the pyrolysis of biomass [5]. In the works of Li et al., cyclopentanone is used as feedstock

* Corresponding author.
E-mail address: niegenkuo@qust.edu.cn (G. Nie).

https://doi.org/10.1016/j.apcatb.2022.122330
Received 14 October 2022; Received in revised form 23 December 2022; Accepted 26 December 2022
Available online 27 December 2022

with/without other carbonyl compounds, such as furfural, 5-hydroxymethylfurfural and chain ketones to synthesize alkyl substituted cyclic hydrocarbons, polycyclic hydrocarbons by combination of aldol condensation and hydrodeoxygenation[6–9]. In the works of Zou et al., cyclohexanone and isophorone are used for self-aldol condensation or aldol condensation with furan aldehydes to produce jet fuels [10,11]. Interestingly, the properties of these fuels have a big difference. Among these fuels, the jet fuel blending synthesized by cyclopentanone and cyclohexanone have the best properties with density range from 0.878 g/mL to 0.940 g/mL and the freezing point lower than − 49 °C, mainly attributing to the mixture fuel compositions, which fully use of the advantages of the properties of each fuel component [2]. Moreover, with consideration of the nature that the lignocellulosic derives pool is a mixture, it is potential to directly obtain the fuel mixture using lignocellulosic derives ketones as feedstock.

To the best of our knowledge, almost all of base, acid and acid-base bifunctional catalysts can catalyze the aldol condensation. Although homogeneous catalysts have significant activity, the drawbacks of separation, corrosion to equipment, no-reusability and being unfriend to the environment stimulate the demand for heterogeneous catalyst. Sensibly, basic metal oxides are sensitive to ambient CO_2 which makes it a challenge to be stable at presence of water [12]. So, solid acid catalysts such as zeolites [13], metallic oxide [9,14], heteropolyacid [15] and resins [2] are emerging as new promising catalyst for aldol condensation. Moreover, due to the hydrodeoxygenation of bio-fuel precursors catalyzed by bifunctional metal/solid acid catalysts are unavoidable for yielding jet fuel [1], it is more significant to develop efficient solid acid for aldol reaction, because it may integrate aldol condensation and hydrodeoxygenation over bifunctional metal-acid catalysts in one pot.

12-phosphotungstic acid (HPW), a Keggin type polyoxometalate is an extremely promising industrial catalyst owing to its strong acid, oxidability and extensive tunability [16,17]. But the surface area is too small (< 5 m^2/g) that it is commonly used as catalysis by supported. Metal oxides, clays, zeolites, mesoporous silica, magnetic materials and MOFs are frequently used as supports [18]. As we all know, HPW is a water-soluble catalyst, and aldol adducts produce water by easily dehydration to enone groups. So, leaching is the unavoidable problem in these HPW supported catalysts in aldol reaction. According to the literature [19], the diameter of the HPW is only 12 Å. So, the pore window of the cage of supports must be adequate small that the HPW particles are confined to inhibit leaching. For instance, pore windows of MIL-101 are 12 Å and 16 Å respectively, so the HPW could be confined in the cage of MIL-101 to make HPW@MIL-101 catalyst reusable in the aldol reaction of ketones [11]. Although MOFs could confine the HPW particles, both the products obtained by this catalyst and the supported amount of HPW are limited. In contrast, zeolites have sufficient and flexible channels and large load capacity. Moreover, it is easy handling to use zeolite as support. For example, 80 % HPW/MCM-41 can be prepared by easy impregnation and is used as an efficient catalyst in the isomerization and dimerization of pinenes and turpentine [20]. Furtherly, in order to prevent the leaching of HPW, a moisture-insensitive zeolite loading catalyst is desired. Alkylimidazole modified SBA-16 creates a relatively hydrophobic environment, which anchors HPW and protects HPW from water [21]. Whereas, grafting of organic functional groups is at the cost of load loss and calcination technology. So, a more appropriate HPW loading method is desirable for the reaction with water presented. Metal salts (Cs^+, Sn^{4+}, Ti^{4+}, Fe^{3+}, Hf^{4+}) of $PW_{12}O_{40}^{3-}$ (MTPA) are water insensitive and exhibit excellent activity in Friedel–Crafts alkylation, esterification, and acylation of aromatic [19]. Metal cations here with electron pair acceptors give Lewis acidity and make MTPA strong acid with both Lewis and Bronsted acids, both of which could catalyze the aldol condensation [12,22,23].

Herein, in order to effectively synthesize high-grade Jet fuel blending precursors by co-aldol condensation of using lignocellulosic ketones mixture directly and taking the reusability of catalyst into consideration, we prepared HfTPA/MCM-41 firstly by co-deposition of $HfCl_4$ and HPW in MCM-41 and this preparation process is simpler and faster than literatures [24]. This catalyst shows good reusability and fuel precursors selectivity than the other commonly used commercial catalysts in the aldol condensation of ketones. After characterization, investigations reveals that the originate of good performance of HfTPA/MCM-41 is ascribed to new L acids produced by dopong Hf the improved surface chemistry properties that efficiently activate C═O bond of ketones to form metal enolate intermediates, leading to the excellent catalytic performance. The introduce of Hf also makes the catalyst water-tolerance and anti-coking, which makes the catalyst reusable. At last, we also demonstrated the general applicability of this catalyst in other biomass-derived carbonyl compounds and realized the efficient co-aldol condensation of lignocellulosic ketones.

2. Experiment

2.1. Materials

Cyclopentanone (AR) and cyclohexanone (AR) were purchased from Shanghai McLean Biochemical Technology Co., LTD and Shanghai Titan Technology Co., LTD respectively. Butyraldehyde (99 %) was obtained from Beijing Minida Technology Co., LTD. Furfural (99 %) was purchased from Qingdao Anlixin Trading Co., LTD. Cycloheptanone (99 %) was obtained from Shanghai Myrell Chemical Technology Co., LTD. Phosphotungstic acid (HPW) was purchased from Shanghai Yuanfan Biotechnology Co., LTD. Hafnium tetrachloride (99.9 %) was purchased from Qingdao Taike Instrument Equipment Co., LTD. Amberlyst-15 resin was purchased from Shanghai Aladdin Biochemical Technology Co., LTD. MCM-41, Hβ (SiO_2/Al_2O_3 = 25), HY (SiO_2/Al_2O_3 = 25), HZSM-5 (SiO_2/Al_2O_3 = 25) and γ-Al_2O_3 were obtained from Tianjin Nankai Molecular Sieve Factory.

2.2. Catalyst preparation

The catalysts were prepared by combination of equivalent-volume impregnation and co-deposition. Here, we show the preparation of 80 %$Hf_{1.5}$TPA/MCM-41 as example and the preparation of other catalysts follows the similar procedure. Before use, MCM-41 was calcinated at 400 °C for 4 h. 2.22 mL 0.12 M HPW solution ($m_{HPW(g)}/m_{MCM\text{-}41(g)}$ = 80 %), 2.22 mL 0.18 M $HfCl_4$ solution ($n_{HfCl4\ (mol)}/n_{HPW\ (mol)}$= 1.5) were mixed and added into the 1 g MCM-41 under stirring until it was formed a viscous consistency. Then the solid was aged at room temperature for 12 h, and dried at 120 °C for 12 h, and calcinated at 300 °C for 3 h. The other loading catalysts (yHf_xTPA/MCM-41, y = ($m_{HfxTPA(g)}/m_{MCM\text{-}41\ (g)}$)*100 %), x = $n_{Hf(mol)}/n_{HPW(mol)}$) are prepared followed the similar approach as above with different loading amounts. Then, Hf_xTPA (x = $n_{Hf(mol)}/n_{HPW(mol)}$) was prepared by co-deposition. Typically, $HfCl_4$ solution was added to HPW solution drop by drop and aged at room temperature for 12 h, and then dried at 120 °C for 12 h, and calcinated at 300 °C for 3 h. 22 %HfO_2/MCM-41 was prepared with loading the same amount of $HfCl_4$ used in the case of 80 %$Hf_{1.5}$TPA/MCM-41. MCM-41 was calcinated at 400 °C for 4 h and other zeolites were calcinated at 580 °C for 3 h before use.

2.3. Catalyst characterization

The crystal structure of catalyst was recorded on a D/MAX/2500PC X-ray diffractometer with (Cu-Kα) radiation. The surface groups of the catalysts were analyzed by Vertex 70 FT-IR spectrometer. The type and amount of acid were determined by pyridine adsorption infrared spectroscopy (PY-IR) and temperature-programmed desorption of ammonia (NH_3-TPD). The acid strength was tested on a Bruker Avance III 500 MHz with a wide aperture spectrometer and the ^{31}P NMR spectra of solid state was obtained by using TMPO as probe molecule and 85 % H_3PO_4 as standard. The acid strength was also tested by Hammett titration on UV-Vis spectrophotometer of a TU-1810 ASPC spectrophotometer. Firstly, 8

mg of Hammett indicator 4-nitrotoluene (pKa = −11.4) was dissolved in 10 mL of toluene and then vigorously stirred for 2 h to obtain the Hammett indicator solution. Then, 20.0 mg of 80 %HPW/MCM-41 or 80 %$Hf_{1.5}$TPA/MCM-41 was dried at 120 °C for 12 h to remove adsorbed water and then placed in 4.0 mL of anhydrous toluene. Followingly, 30.0 μL of Hammett indicator solution was added to the above catalysts respectively and stirred for 6 h and then the catalysts were centrifuged to move out. Finally, the solution was tested by UV-Vis spectrophotometer [25]. X-ray photoelectron spectroscopy (XPS) was used to measure the surface chemical environment of the sample on Thermo Fisher ESCALAB XI^+ equipped with an Al Kα X-ray source (1486.6 eV). The morphology of the samples was observed by transmission electron microscopy (TEM) of JEM-F200. The porous structure of the catalyst was tested by the N_2 adsorption and desorption at the Micomeritics ASAP 2020 volumetric adsorption analyzer. Typically, 0.1 g catalyst was firstly degassed under vacuum of < 5 Pa at 250 °C for 10 h before test. The specific surface areas of catalysts were calculated by the Brunauer-Emmett-Teller (BET) equation and the pore volume was calculated by the Barrett Joyner-Halenda (BJH) equation. Thermogravimetric (TG) test was carried out on a NETZSCH TG209F1 at a heating rate of 10 °C/min and temperatures ranging from 30 °C to 900 °C. A water contact angle test for the catalysts was conducted using a JC2000D1. The contents of elements were analyzed by inductively coupled plasma (ICP) on Agilent ICP-OES730.

2.4. Catalytic reaction and product analysis

The aldol condensation of cyclopentanone and cyclohexanone was conducted in a 25 mL three-necked round-bottom flask. Typically, 2.00 g cyclopentanone, 2.33 g cyclohexanone and 0.43 g catalyst were added into the flask, and the reaction was conducted at 130 °C for 4 h. The conversion of lignocellulosic ketones pool over 80 %$Hf_{1.5}$TPA/MCM-41 was conducted in a 25 mL three-necked round-bottom flask. 0.34 g 80 % $Hf_{1.5}$TPA/MCM-41 and 3.40 g lignocellulosic ketones (the composition as depicted in the Scheme 1) were used in this reaction. Firstly, cycloheptanone, butyraldehyde, cyclopentanone (half amount) and cyclohexanone (half amount) were added into the reactor with catalyst for reaction at 150 °C. After 10 h, the temperature was reduced to 100 °C and the remaining feedstock was added to react for 6 h. Here, temperature gradient reaction is a good method to increase the product yield, considering the sensitivity of the reactants to temperature. The reaction products were analyzed by a gas chromatography (GC-2010 PRO) equipped with an FID detector and a DB-5 capillary column (30 m × 0.32 mm × 0.25 μm) and an Agilent 7890B/5975 C gas chromatography mass spectrometer (GC-MS) equipped with an HP-5 capillary column (30 m × 0.32 mm × 0.25 μm). The temperature was started from 50 °C and stated for 1 min and raised to 280 °C at a rate of 10 °C/min and was held at 280 °C for 5 min

3. Results and discussion

3.1. Catalyst characterization

Characterizations were conducted to recognize the morphology and structure of the synthesized HfTPA/MCM-41 catalysts. The XRD patterns of y$Hf_{1.5}$TPA/MCM-41 and 80 %Hf_xTPA/MCM-41 are displayed in Fig. 1a and Fig. 1b, respectively. The broad peak at 2θ = 15–40∘ is the peak of MCM-41, which is broadened with the increasing loading amount of $Hf_{1.5}$TPA, meanwhile all the samples with loading amount no more than 80 % keep the hexagonal meso-structure by the diffraction peaks exhibited at 2θ = 2∘ (100) and 2θ = 3–6∘ (belonging to the (110) and (200) reflexes respectively), which suggests appropriate loading amount of Hf_xTPA will not destroy the ordered hexagonal mesoporous structure of MCM-41. Smooth peaks at 2θ= 8, 19, 27 and 35∘ referring

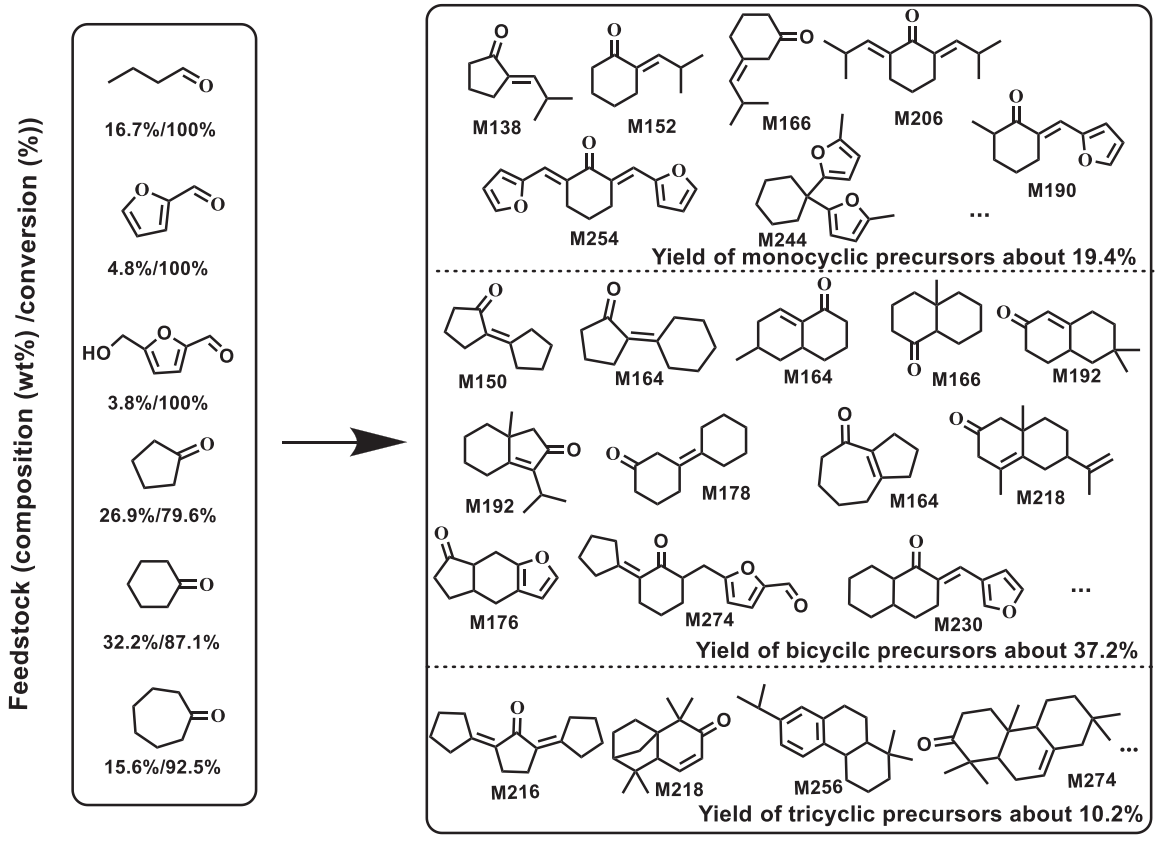

Scheme 1. Aldol condensation of lignocellulosic ketones mixture to Jet fuel precursors over 80 %$Hf_{1.5}$TPA/MCM-41.

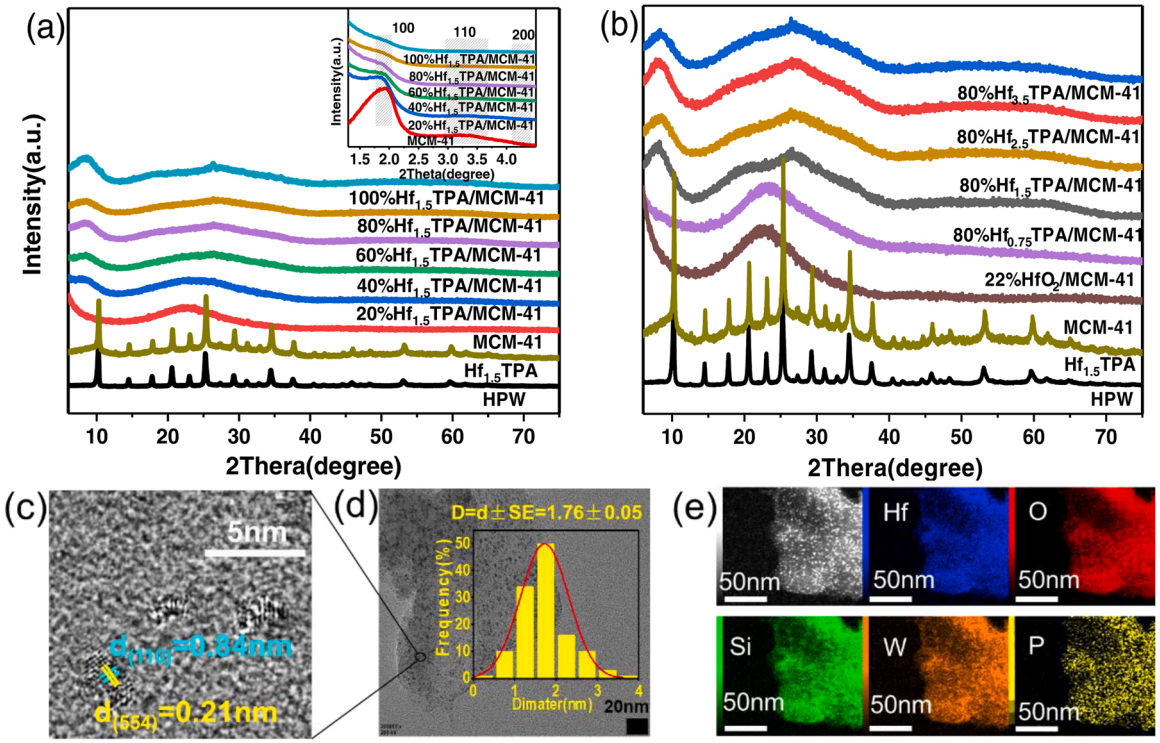

Fig. 1. XRD results of y$Hf_{1.5}$TPA/MCM-41 catalysts (a) and 80 %Hf_xTPA/MCM-41 catalysts (b). The HAADF STEM image (c), TEM images (d) and EDX mapping results (e) of 80 %$Hf_{1.5}$TPA/MCM-41.

to $Hf_{1.5}$TPA begin to appear as the loading amount of $Hf_{1.5}$TPA exceeds 80 %, which indicates $Hf_{1.5}$TPA uniformly distributed in the samples with $Hf_{1.5}$TPA loading amount no more than 80 %. Interestingly, changing the ratio of Hf to HPW could cause different degrees of agglomeration of the supported particles. As only $HfCl_4$ was supported, catalysts present similar characteristic peaks between 80 % HfO_2/MCM-41 and MCM-41. As loading the coprecipitate of $HfCl_4$ and HPW, characteristic peaks of HfxTPA appear and clear sharp peaks formed for 80 % $Hf_{3.5}$TPA/MCM-41, indicating agglomeration appeared. As for the catalyst 80 %$Hf_{1.5}$TPA/MCM-41, the lattice spacings of 0.21 nm and 0.84 nm presented in the HAADF results (Fig. 1**c**) are corresponded to the (554) and (110) crystal plane of $Hf_{1.5}$TPA respectively [26]. After loading $Hf_{1.5}$TPA, there is no obvious change to the MCM-41 from the TEM images (Fig. S1). The sizes of $Hf_{1.5}$TPA nanoparticle calculated by the Scherrer equation are smaller than 5 nm, which is further confirmed by the size distributions obtained from TEM images with a uniform radius of about 1.76 nm observed (Fig. 1**d**). Moreover, from the EDX mapping (Fig. 1**e**), the uniform distribution of Si, W, O, P and Hf further confirms a well dispersion of $Hf_{1.5}$TPA in MCM-41.

The textural parameters of catalysts are shown in Table 1. MCM-41 has the highest specific surface area about 971 m^2/g, while the lowest one is $Hf_{1.5}$TPA of 1 m^2/g. With the increasing loading amount of $Hf_{1.5}$TPA, surface area, pore diameter, and volume of catalysts decrease. Interestingly, the surface area of 80 %$Hf_{1.5}$TPA/MCM-41 is higher than 80 %HPW/MCM-41, while both the pore diameter and volume are smaller, suggesting the successful introduction of $Hf_{1.5}$TPA nanoparticles into the channels of MCM-41. According to N_2 adsorption and desorption isotherms (Fig. S2a), all $Hf_{1.5}$TPA/MCM-41 catalysts show type IV Langmuir isotherms, signifying mesoporous structure kept and the sizes distributions of pores display a significant peak at about 3–4 nm based on the BJH method for the adsorption branch (Fig. S2b). 80 %$Hf_{1.5}$TPA/MCM-41 has the similar surface area, volume and diameter with Hβ, of which the surface area is less and the volume and diameter are bigger than HY and HZSM-5 (Table 1 **and** Fig. S2c). Amberlyst-15 has the smallest surface area, while the volume and dimer are the biggest.

Table 1
The surface area, volume and diameter of catalysts by N_2 adsorption and desorption characterization.

Catalyst	S_{BET} (m^2/g)	V_P (cm^3/g)	D (nm)
HPW [27]	4	0.18×10^{-2}	2.80
Hβ	494	0.41	3.32
Amberlyst-15 [2]	4	0.40	30.00
HY	666	0.38	2.29
HZSM-5	341	0.18	2.17
$Hf_{1.5}$TPA	1	0.03×10^{-3}	1.20
MCM-41	971	0.99	4.10
80 %HPW/MCM-41	415	0.41	3.95
22 %HfO_2/MCM-41	848	0.83	3.95
20 %$Hf_{1.5}$TPA/MCM-41	735	0.73	3.97
40 %$Hf_{1.5}$TPA/MCM-41	600	0.58	3.88
60 %$Hf_{1.5}$TPA/MCM-41	487	0.46	3.79
80 %$Hf_{1.5}$TPA/MCM-41	430	0.40	3.75
100 %$Hf_{1.5}$TPA/MCM-41	368	0.34	3.68

The FI-IR spectra of samples are exhibited in the Fig. 2 and ball-and-stick model of HPW is shown in Fig. S3. The strong peak at 1080 cm^{-1} is associated with the P-O_a band, and the strong peaks at 814 cm^{-1}, 985 cm^{-1} and weak peak at 890 cm^{-1} are belonged to W-O_c-W, W-O_d and W-O_b-W bands respectively, indicating the Keggin anions of HPW. The peak at 1600 cm^{-1} indicates the presence of protonic acid, which also corresponds to the strong Bronsted (B) acidity of phosphotungstic acid [27,28]. As the doping of Hf, the Hf-O bands are formed with new strong peaks at 600 cm^{-1} (Si-O-Hf) [29], 1560 cm^{-1} (O-Hf-O) [30] and 741–923 cm^{-1} (W-O-Hf) [31] appeared, which are presented in the spectra of HfO_2, $Hf_{1.5}$TPA, 80 %HfO_2/MCM-41 and $Hf_{1.5}$TPA/MCM-41 but 80 %HPW/MCM-41, signifying the Hf species has loaded on the $Hf_{1.5}$TPA/MCM-41. Furthermore, there is a red shift of the W-O_d band after Hf doping, also indicating an effect of Hf on Keggin anions. Moreover, the band at 3300 cm^{-1} could be assigned to the Hf-OH [32]. Then, the ^{31}P MAS NMR spectra of 80 %HPW/MCM-41 % and 80 %

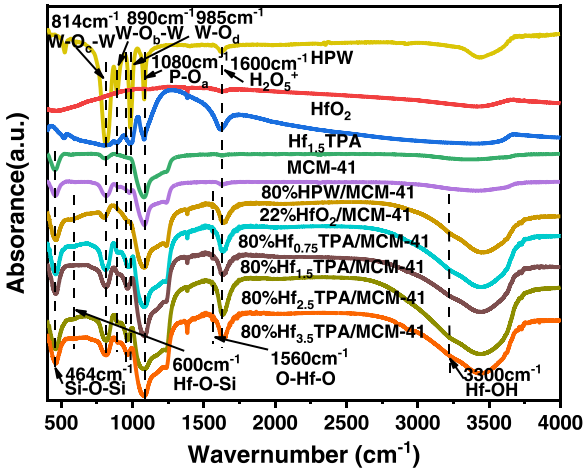

Fig. 2. FT-IR spectra of catalysts.

$Hf_{1.5}$TPA/MCM-41 are compared and analyzed (Fig. 3**a**). All the catalysts exhibit a major peak at about − 15.7 ppm corresponding to the tetrahedral coordination of PO_4 in Keggin unit [20], while a shoulder peak at − 31.5 ppm accounting for the interaction between Keggin anions and Hf. This interaction can also be confirmed by the XPS spectra of catalysts (Fig. 3b, c, d and Fig. S4). For W 4f spectra of 80 % HPW/MCM-41, the doublets at 35.8 and 38.0 eV are ascribed to W^{6+} species. As for the 80 %$Hf_{1.5}$TPA/MCM-41 catalyst, the double peaks at 34.9 and 37.0 eV are ascribed to W^{5+} species[33,34], and the ratio of W^{6+} spectra is bigger. The new spectra are attributed to the effect of Hf species, that the spectra of Hf 4 f are split to four spectra with peaks at 18.8 eV and 17.2 eV attributing to Hf 4f5/2 and Hf 4f7/2 respectively assigning to Hf–O bands and peaks at 19.6 eV and 17.9 eV belonging to Hf–O–W mix phase bonding peak. The Hf–O–W phase formation could also be confirmed from the deconvolution of O 1 s peaks, that peaks at 529.3 eV due to Hf–O bond (Hf^{4+} species), at 532.6 eV due to oxygen vacancy and one more peak at 531.0 eV assigned to mix phase Hf–O–W (Hf^{2+} species) [35]. Because of the oxygen defect, these W^{5+} and Hf^{2+} active sites also could act as Lewis (L) acids and catalyze the aldol reaction of ketones. Additionally, the similar bonding energies of W-O-P and Si-O-Si bonds of 80 %HPW/MCM-41 and 80 %$Hf_{1.5}$TPA/MCM-41 and the red shift of W-O-W bond from 531.0 eV of 80 %HPW/MCM-41 to 531.4 eV of 80 %$Hf_{1.5}$TPA/MCM-41, suggesting Hf species really interact with HPW on MCM-41.

The acid properties of the catalysts were measured by NH_3-TPD, Py-FTIR, ^{31}P solid-state NMR and Hammett test. According to Table 2, HPW has acid amount about 0.96 mmol/g, and $Hf_{1.5}$TPA has acid amount about 0.81 mmol/g. This may be because the $Hf_{1.5}$TPA has agglomerated that the amount of surface acids decreases. As it was supported on the MCM-41, the acid amount increases along with the loading amount of $Hf_{1.5}$TPA, especially the medium and strong acids. With the Hf percentage in the 80 %Hf_xTPA/MCM-41 increasing, weak acids slightly decrease while medium and strong acids firstly increase and then

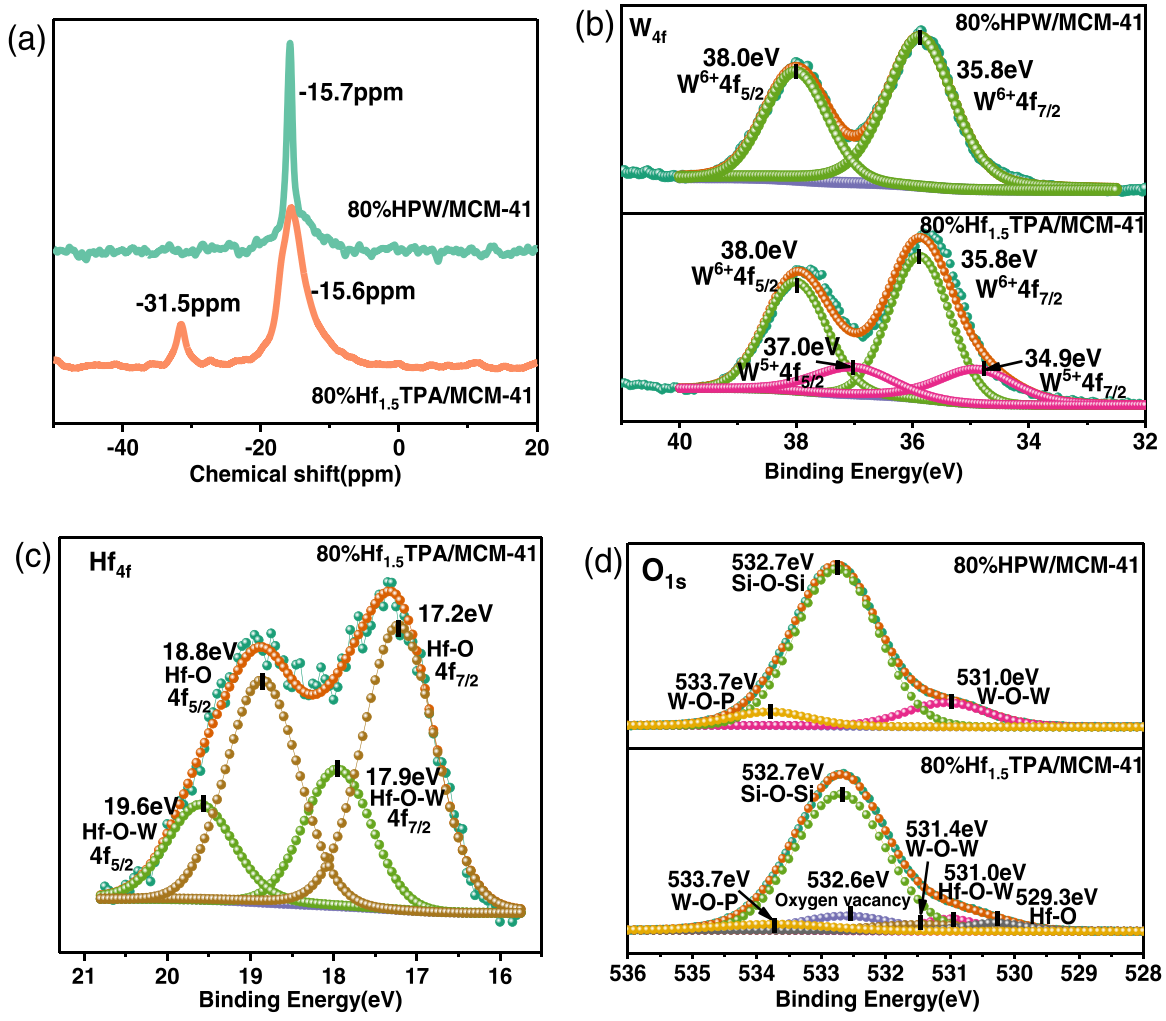

Fig. 3. ^{31}P MAS NMR (a) and XPS spectra (b-d) of 80 %HPW/MCM-41 and 80 %$Hf_{1.5}$TPA/MCM-41.

Table 2
The acid properties of the catalysts.

Sample	Acid amount by NH_3-TPD ($mmol \cdot g^{-1}$)				Acid amount by pyridine FT-IR ($mmol \cdot g^{-1}$)		
	Weak	Medium	Strong	Total	Strong L	Total L	B/L
γ-Al_2O_3	0.29	-	0.29	0.51	0.04	0.20	0.28
HY	0.37	0.33	0.86	0.86	-	-	-
Hβ	0.19	0.33	0.45	0.97	-	-	-
HZSM-5	0.14	0.46	0.42	1.02	-	-	-
Amberlyst-15 [2]	-	-	-	4.13	-	-	-
MCM-41	0.16	0.18	0.20	0.54	-	-	-
HPW	0.34	-	0.84	0.96	-	-	-
$Hf_{1.5}TPA$	0.11	0.15	0.55	0.81	-	-	-
80 %HPW/MCM-41	0.19	0.19	0.54	0.92	0.01	0.17	7.2
22 %HfO_2/MCM-41	0.24	0.42	0.23	0.89	0.13	0.43	0.1
20 %$Hf_{1.5}TPA$/MCM-41	0.28	0.35	0.11	0.74	-	-	-
40 %$Hf_{1.5}TPA$/MCM-41	0.34	0.48	0.15	0.96	-	-	-
60 %$Hf_{1.5}TPA$/MCM-41	0.37	0.64	0.16	1.17	-	-	-
80 %$Hf_{0.75}TPA$/MCM-41	0.18	0.19	0.74	1.11	0.12	0.20	4.3
80 %$Hf_{1.5}TPA$/MCM-41	0.19	0.23	0.79	1.21	0.13	0.22	3.2
80 %$Hf_{2.5}TPA$/MCM-41	0.11	0.15	0.80	1.06	0.13	0.22	2.3
80 %$Hf_{3.5}TPA$/MCM-41	0.12	0.15	0.81	1.08	0.17	0.29	2.0
100 %$Hf_{1.5}TPA$/MCM-41	0.35	0.75	0.17	1.26	-	-	-

decrease with 80 %$Hf_{1.5}TPA$/ MCM-41 having the biggest amount (1.21 mmol/g) acids in the 80 %Hf_xTPA/ MCM-41 catalysts. Compared the acid amounts of 80 %$Hf_{1.5}TPA$/MCM-41 (1.21 mmol/g), 80 %HPW/MCM-41 (0.92 mmol/g) and 22 %HfO_2/MCM-41 (0.89 mmol/g), doping Hf to the HPW/MCM-41, acid amount increases, especially the medium and strong acids. Then, the acid types of the catalysts were also analyzed. As shown in Fig. S5 and Table 2, the peaks at 1446, 1596 and 1611 cm^{-1} are assigned to the Lewis (L) acids, and the peaks at 1539, 1634, 1650 cm^{-1} are belonged to the Bronsted (B) acids, while the peak at 1486 cm^{-1} belongs to an overlap of B and L acids. The peak intensities at 1446 cm^{-1} increases significantly when the doping amount of Hf increases from 80 %HPW/MCM-41 to 80 %$Hf_{3.5}TPA$/MCM-41, indicating that the Hf is the main source of L acids (in consistence with the XPS result), especially the strong L acid. In addition, the B/L molar ratio decreases from 7.2 in the case of 80 %HPW/MCM-41 to 0.1 in the case of 22 %HfO_2/MCM-41. The acid strength of the catalysts was characterized by ^{31}P solid-state NMR in Fig. 4. Three characteristic peaks are found by Gaussian simulation at 67 ppm (26.8 %), 77 ppm (44.7 %) and 87 ppm (28.5 %) in ^{31}P MAS NMR spectra of 80 %HPW/MCM-41, which belong to weak, strong, and super-strong B acids respectively [36,37]. After Hf doping, peaks shift and split with new peaks at 65 ppm (6.7 %), 70 ppm (10.3 %) belonging to the new L acids and 95 ppm (15.5 %) attributing to superacid, suggesting the Hf doping not only can create L acid (in consistence with the XPS result and Py-FTIR result) but also improve the acid strength. Although some peaks (60 ppm of 33.3 %) have blue shifted, they are still more than 60 ppm. In order to further confirm the catalyst strength, we used concentration change of Hammett indicator tested by UV-Vis spectrophotometer to calculate the H_0 values of the catalysts [38]. From Fig. 4b, after catalysts adsorption, the spectra intensity of the remained Hammett indicator by 80 %$Hf_{1.5}TPA$/MCM-41 is weaker than 80 %HPW/MCM-41 with the Hammett index of 80 %$Hf_{1.5}TPA$/MCM-41 about − 13.23 and the 80 %HPW/MCM-41 about − 12.64 (Table S1). The weaker the spectra the lower the value of H_0 and the stronger the catalyst acid [39], confirming the doping Hf improving the catalyst acid strength.

3.2. *Efficient activity of catalyst in aldol reaction*

The catalytic performance of the 80 %$Hf_{1.5}TPA$/MCM-41 in aldol reaction of cyclohexanone and cyclopentanone was evaluated at 130 °C and compared the results with other commercial catalysts. In this reaction, primary condensation (C_5-C_5, C_5-C_6, C_6-C_6) and secondary condensation of ketones (C_5-C_5-C_6, C_6-C_5-C_6) are the main products (Fig. 5a and Fig. S6). Along with the time, the secondary condensation products increase while the primary condensation products decrease slightly, meaning that secondary condensation products are formed based on the consumption of the primary condensation products with the products content of C_6-C_6-C_5 > C_5- C_6 = C_5-C_5-C_6 > C_6-C_6 > C_5-C_5 at

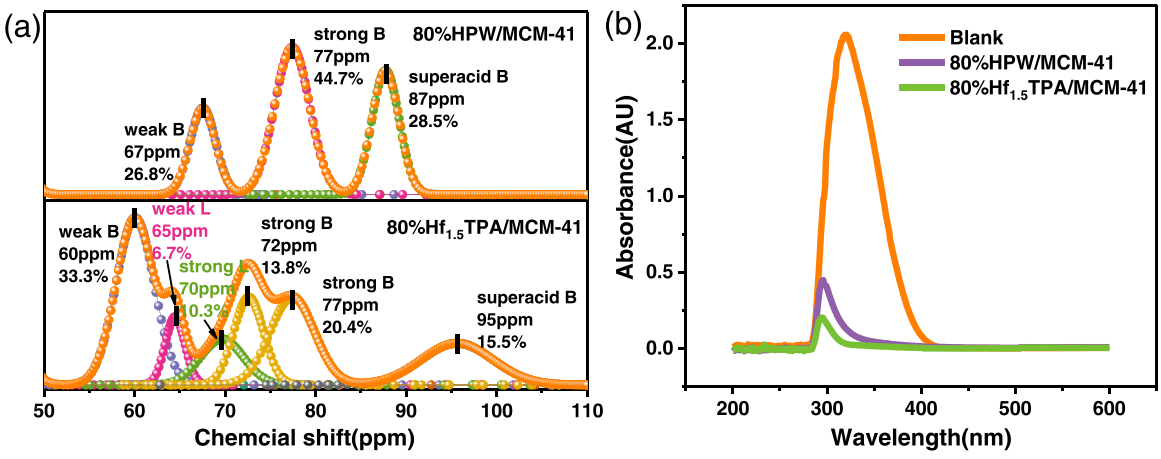

Fig. 4. ^{31}P MAS NMR spectra of protonated TMPO on 80%HPW/MCM-41 and 80 %$Hf_{1.5}TPA$/MCM-41 (a). UV-Vis spectra of 4-nitrotoluene after 80 %HPW/MCM-41 and 80 %$Hf_{1.5}TPA$/MCM-41 adsorption (b).

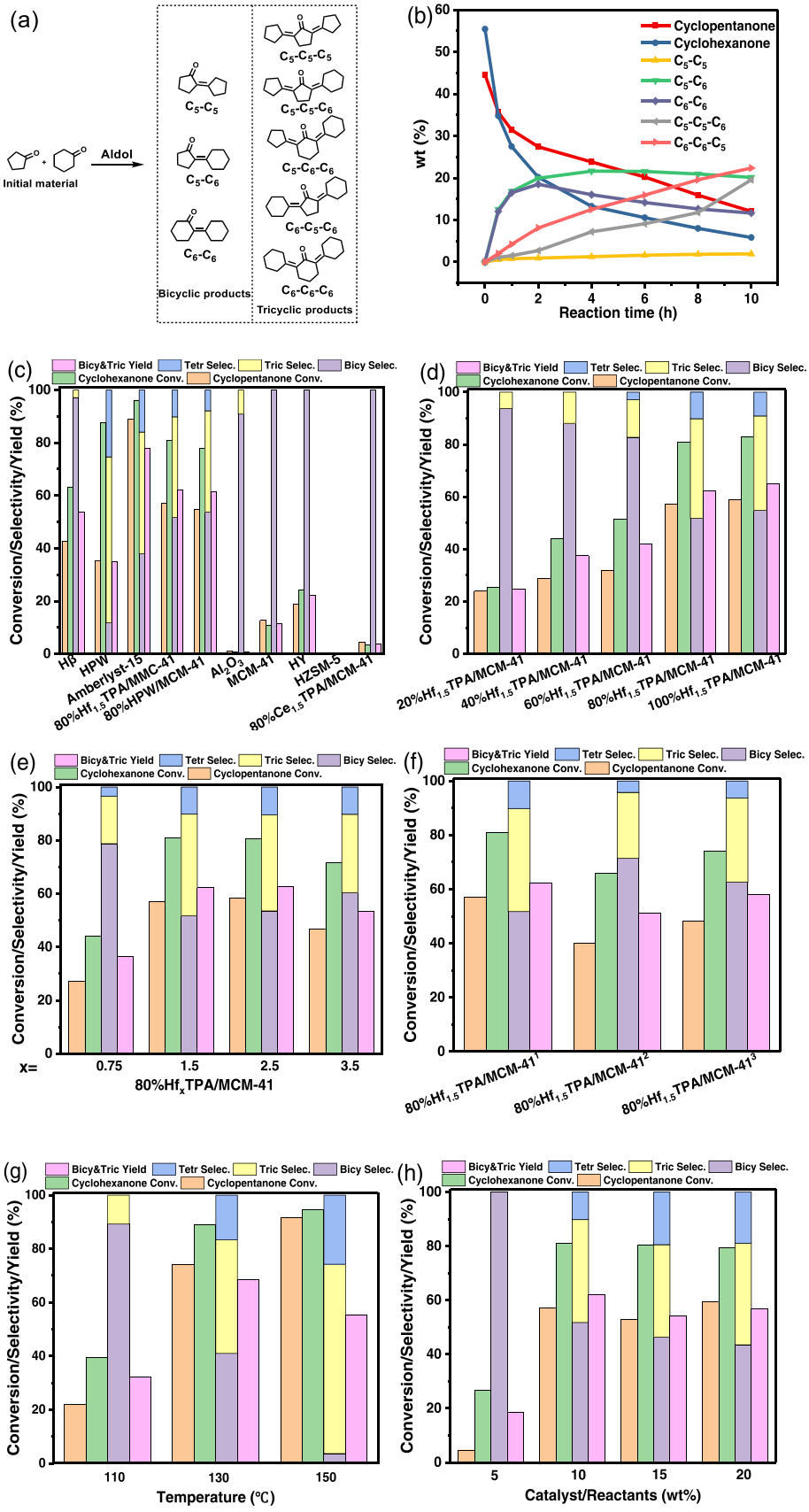

Fig. 5. The scheme of reaction of cyclopentanone with cyclohexanone (a). The reaction trend of cyclopentanone and cyclohexanone (b). The effects of different catalysts (c), loading amount (y$Hf_{1.5}$TPA/MCM-41) (d), ratios of Hf to HPW (80 %Hf_xTPA/MCM-41) (e), catalyst prepared methods (f), temperature(g) and the catalysts amount (h) to the reaction. Reaction conditions: 2.00 g cyclopentanone, 2.00 g cyclohexanone, 4 h. The preparation of 80 % $Hf_{1.5}$TPA/MCM-41[1], 80 %$Hf_{1.5}$TPA/MCM-41[2], 80 % $Hf_{1.5}$TPA/MCM-41[3] was illustrated in the supporting information.

10 h (Fig. 5b). Due to primary and secondary condensation products can make high-performance fuel blending. Here, we take the sum of both as the target products of the reaction.

As illustrated in Fig. 5c, Amberlyst-15 has the highest product yield, but it cannot be reused after coking. The product yield of 80 %$Hf_{1.5}$TPA/MCM-41 is a little higher than that of 80 %HPW/MCM-41, and they are much higher than HPW and commercial zeolites, such as Hβ, Al_2O_3, MCM-41, and HZSM-5. HZSM-5 has almost no activity in this reaction because its pores are too small (Table 1). The conversion of ketones by Al_2O_3 is also poor, because the acid strength of Al_2O_3 is weak (Table 2). With pore size increases, the yield of products increases from HZSM-5 to HY and then Hβ, indicating pore size plays an important role in products formation. As shown in the Table 1, the surface area of HPW is only 4 cm^2/g, and as it is supported on the MCM-41, the amount of the efficient acids increases resulting a bigger yield of products. As doping Hf, Hf changes the electronic structure of the catalyst surface (see the XPS result), which makes 80 %$Hf_{1.5}$TPA/MCM-41 has more medium and strong acids, especially L acids than 80 %HPW/MCM-41 (see Table 2 and Fig. 4), so the product yield also increases, indicating that doping Hf efficiently activate C═O bond of ketones to form a metal enolate intermediate to improve the catalyst catalytic performance [12]. Then, the effects of loading amounts of $Hf_{1.5}$TPA are tested in the aldol condensation of cyclohexanone and cyclopentanone (Fig. 5d). Products yields increase with the loading amount of $Hf_{1.5}$TPA, and when the loading amount of $Hf_{1.5}$TPA increases to more than 80 %, the increasing trend is not obvious. This is because the acid amount increases along with the loading amount of $Hf_{1.5}$TPA while the surface area decreases (Table 1), which leads to the efficient acids amount increasing and then decreasing (Table 2). We also investigated the effects of Hf/HPW ratio on the reaction. As shown in Fig. 5e, with the ratio of Hf increases from x = 0.75 to x = 3.5 of 80 %Hf_xTPA/MCM-41, the products yields increase from 36.4 % (80 %$Hf_{0.75}$TPA/MCM-41) to 62.2 % (80 %$Hf_{1.5}$TPA/MCM-41) and 62.7 % (80 %$Hf_{2.5}$TPA/MCM-41) and then decreases to 53.4 % (80 %$Hf_{3.5}$TPA/MCM-41). This change is tightly associated with the total acid amount, especially the increasing of L acids (Table 2), indicating that L acid is an efficient active site for aldol condensation. Then, the effects of loading sequence of Hf and HPW on MCM-41 in preparation of catalysts to catalyst activity are investigated and the products yields of the catalysts are compared. As shown in Fig. 5f, there is no obvious difference among products yields of these catalysts. At last, the influence of the temperature on the reaction is investigated. As shown in Fig. 5g, too low temperature cannot stimulate the reaction and the product yield increases with the temperature. But too high temperature motivates the reaction to proceed more secondary condensation of ketones, even with the formation of polymeric compounds. So, the product yield at 150 °C is only 55 %, which is lower than the one at 130 °C (68 %). Also, the effect of the mass ratio of catalyst to reactants in the reaction is also analyzed. As presented in the Fig. 5h, as the mass ratio of catalyst to reactants increases to 10 %, the conversion of ketones and the products yield level off.

3.3. The water-tolerance of HfTPA/MCM-41 in aldol reaction

As we all know, water is unfriendly to the acid reaction, especially the leaching effect for the loading acid catalyst. As shown in Fig. 6a, the conversion of ketones and product yields by 80 %$Hf_{1.5}$TPA/MCM-41 and 80 %$Hf_{2.5}$TPA/MCM-41 are comparable. Here, as equimolar water produced by aldol condensation of ketones was added before the reaction, the reaction result by 80 %$Hf_{1.5}$TPA/MCM-41 has been slightly improved while the result by 80 %$Hf_{2.5}$TPA/MCM-41 has been slightly weaken (Fig. 6a). But both have no obvious change before and after water feeding, indicating a little water has no influence on the activity of 80%Hf_xTPA/MCM-41. Then, 80%HPW/MCM-41 and 80 %$Hf_{1.5}$TPA/MCM-41 were washed by water for 5 h using soxhlet extraction and then dried and calcinated following the same procedure of catalyst preparation. The obtained catalysts were used in the reaction and the conversion of ketones and product yields are compared in Fig. 6b. Obviously, both conversion of ketones and products yield decrease and no more than 8 % yield of product by 80 %HPW/MCM-41 while more than 30 % yield of product by 80 %$Hf_{1.5}$TPA/MCM-41 are obtained, indicating the stability of the loaded HPW has been improved by Hf doping on the MCM-41. This result can also be confirmed by the elements contends analysis by ICP in Table 3. After water washing, both catalysts have the same molar ratio of W/P about 12, which is the same with the element contents in Keggin unit. Compared with the fresh catalysts, Si and Hf contents keep the same, while P/Si content in 80 %HPW/MCM-41 decreases much more obvious than that in 80 %$Hf_{1.5}$TPA/MCM-41, meaning the doping Hf could improve the stability of Keggin unit on MCM-41. However, compared with the fresh catalyst, Hf/P content increases. Maybe some isolated Keggin units have not integrated with Hf and they are sectionally dissolved into water. Moreover, the better suspension state of catalysts in water and increasing water contact angle of the samples with doping Hf increasing presented in Fig. S7 confirm that Hf doping could increase the hydrophobicity of HPW loading samples.

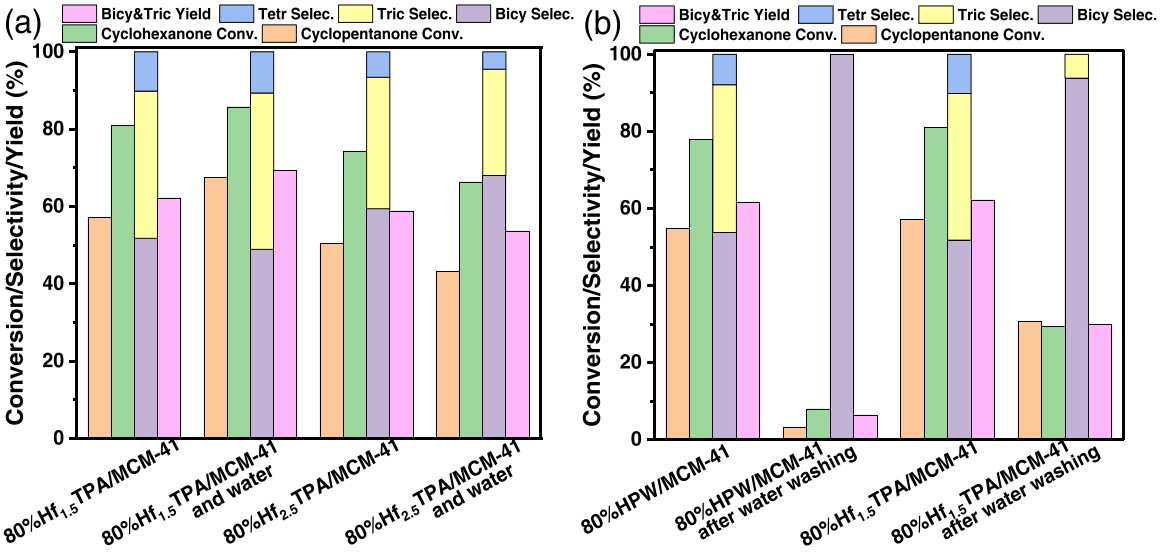

Fig. 6. The effects of added water (a) and the washing procedure of catalysts (b) to the reaction. Reaction conditions: 2.00 g cyclopentanone, 2.00 g cyclohexanone, 0.43 g catalyst, 130 °C, 4 h.

Table 3
Elements contents of catalysts measured by ICP.

Sample	wt %)				Mol/mol		
	Hf	P	W	Si	W/P	Hf/P	Si/P
80 %HPW/MCM-41	-	0.43	29.69	10.54	11	-	37
80 %HPW/MCM-41 After 5 h	-	0.01	0.89	13.97	12	-	437
80 %$Hf_{1.5}$TPA/MCM-41	3.54	0.37	27.26	12.64	12	2	36
80 %$Hf_{1.5}$TPA/MCM-41 After 5 h	2.85	0.03	2.38	15.19	12	11	190

3.4. The anti-coking properties of HfTPA/MCM-41 in aldol reaction

The reusability of the catalyst is important for the reaction, especially for the potential of industrialization. Here, 80 %HPW/MCM-41 and 80 %$Hf_{1.5}$TPA/MCM-41 were tested in continuous reactions to compare the reusability. As depicted in the Fig. 7, 80 %$Hf_{1.5}$TPA/MCM-41 can be used twice stably and then the conversion and products yield decrease in reaction after reaction, and products yield decreases to 43 % in the fourth run which is much higher than that (12.4 %) by 80 %HPW/MCM-41 in the fourth run. This result demonstrates the doping Hf can improve the stability of catalyst by preventing the leaching of Keggin unit from the MCM-41, which could be speculated from the elements content change by ICP result (Table 3) that Si/P mol ratio of 80 %HPW/MCM-41 (437) is much bigger than that of 80 %$Hf_{1.5}$TPA/MCM-41 (190) after being washed. In addition, the coke is also an important influence factor for the catalyst reusability. As shown in Fig. 8 and Table S2, after once reaction, the mass loss of 80 %HPW/MCM-41 by TG is about 7.0 % compared with the fresh one while the mass change of 80 %$Hf_{1.5}$TPA/MCM-41 is 5.2 %, indicating that the Hf doping can prevent the coke formation. However, after the fourth reaction, the mass loss of 80 %HPW/MCM-41 is only 6.1 % compared with the fresh one, while the mass change of 80 %$Hf_{1.5}$TPA/MCM-41 is 9.7 %. This is because the HPW leaching occurs (ICP result in Table 3) on 80 %HPW/MCM-41, that mass loss of 80 %HPW/MCM-41 after the fourth run is − 0.9 % compared with that of the twice run. Lastly, the thermostability is also important for the catalyst reusability, that the fresh 80 %HPW/MCM-41 began to decompose at 461 °C and the fresh 80 %$Hf_{1.5}$TPA/MCM-41 began to decompose at 480 °C, suggesting that the Hf doping can improve the thermostability of the catalysts.

3.5. The expanding application of 80 %$Hf_{1.5}$TPA/MCM-41 in aldol condensation of more ketones

Due to the good products yield of condensation of cyclohexanone and cyclopentanone by 80 %$Hf_{1.5}$TPA/MCM-41, condensation of more ketones was investigated using 80 %$Hf_{1.5}$TPA/MCM-41 as the catalyst. As shown in Table 4, all the ketones can be converted to primary and secondary condensed products in self-condensation. Interestingly, the conversion of these ketones follows in order as $C_{cyclopentanone}$ (68.4 %, **entry 1**) > $C_{cyclohexanone}$ (63.5 %, **entry 2**) > $C_{cycloheptanone}$ (52.0 %, **entry 3**) > $C_{5\text{-}HMF}$ (47.2 %, **entry 4**), while the products yield follows in the order of $Y_{cyclohexanone}$ (59.5 %, **entry 2**) > $Y_{cycloheptanone}$ (51.1 %, **entry 3**) > $Y_{cyclopentanone}$ (48.4 %, **entry 1**). This is because small cyclic ketones are easily activated over the solid acid sites and proceed further condensation that more deep condensed products are produced from cyclopentanone meanwhile steric hindrance prevents condensation of macrocyclic ketone. Reasonably, the highest products yield is obtained from condensation of cyclohexanone and slightly lower products yield is obtained from condensation of cyclopentanone and cycloheptanone. Due to there will no cyclic hydrocarbon precursors by self-condensation of 5-HMF, the product yield is 0. In the cross condensation of cyclopentanone with other ketones, the conversion of cyclopentanone increases except for the condensation of cyclopentanone and butyraldehyde. This may be because the metastable intermediate by the cross condensation of cyclic ketones decreases the energy barrier of the reaction[40] while over condensation products cover the acid sites in the condensation of cyclopentanone with butaldehyde[41].

Given the mixture of lignocellulosic derivatives into consideration, ketones pool was catalyzed in one-pot reaction is more valuable in real production. Herein, we used 80 %$Hf_{1.5}$TPA/MCM-41 as catalysis to catalyze the condensation of ketones pool and the results are shown in the Scheme 1 and Fig. S8. All the ketones are almost converted completely with about 66.8 % of total products yield obtained (19.4 % of monocyclic compounds, 37.2 % of bicyclic compounds and 10.2 % of tricyclic compounds). This result demonstrates that 80 %$Hf_{1.5}$TPA/MCM-41 is an efficient catalyst for co-conversion of lignocellulosic derived ketones. Moreover, there are many new compounds produced, compared with the products in Table 4, attributing to the more kinds of feedstock the more complex of reaction.

4. Conclusion

We synthesized a strong solid acid catalyst 80 %$Hf_{1.5}$TPA/MCM-41 with high stability and used it to synthesize high-performance bio-jet fuel blending precursors by co-aldol condensation of lignocellulosic

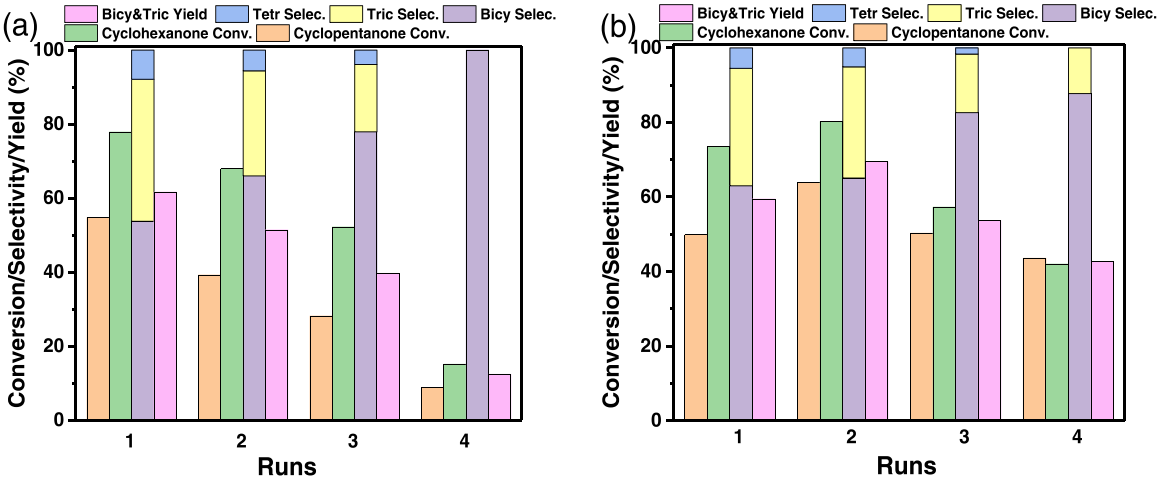

Fig. 7. Reusability of 80 %HPW/MCM-41 (a) and 80 %$Hf_{1.5}$TPA/MCM-41(b). Reaction condition: 2.00 g cyclopentanone, 2.00 g cyclohexanone,0.43 g catalyst, 130 °C, 4 h.

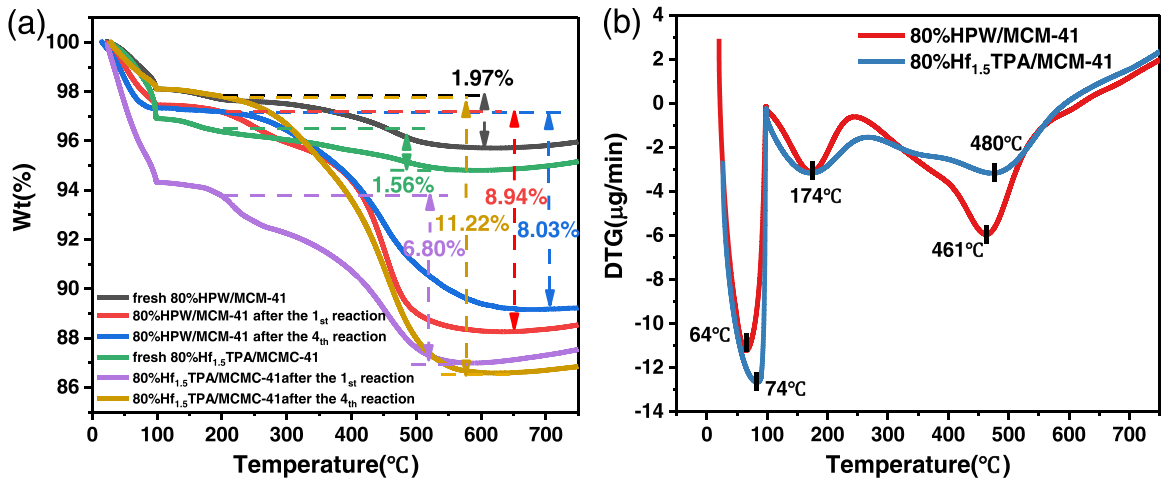

Fig. 8. TG (a) and DTG (b) curves of 80 %HPW/MCM-41 and 80 %$Hf_{1.5}$TPA/MCM-41.

Table 4
C-C coupling reactions catalyzed by 80 %$Hf_{1.5}$TPA/MCM-41.

Enty	Substrates	Conversion (%) in this work/ literature	Products yield (%) in this work/ literature	Reaction condition in this work/ literature
1	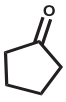	68.4/46.4 [11]	48.4/45.5	150 °C, 8 h/ 130 °C, 48 h
2	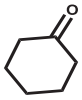	63.5/48.0 [11]	59.5/47.0	150 °C, 8 h/ 130 °C, 24 h
3	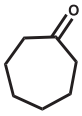	52.0/10.0 [11]	51.1/9.0	150 °C, 10 h/ 130 °C, 48 h
4[a]	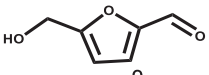	47.2/-	0/-	60 °C, 6 h/-
5	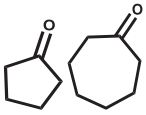	82.0, 50.8/-	58.9/-	150 °C, 10 h/-
6	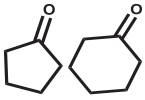	57.0, 80.9/ 90.0, 100.0 [2]	62.1/82.0	130 °C, 4 h/ 100 °C, 12 h
7	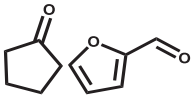	66.8, 95.9/ -, 80.0[42]	43.2/60.0	60 °C, 6 h/ 60 °C, 6 h
8	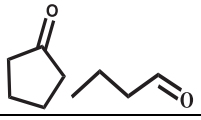	45.0, 99.7/ -,99.0[41]	47.0/63.0	150 °C, 8 h/ 140 °C, 4 h

[a] Due to no potential cyclic compound formation in this reaction, there is no objective products yield obtained.

derivatives ketones. This catalyst has strong acid, big acid content and especially highly improved stability compared with HPW/MCM-41 and presents an excellent activity better than commercially used zeolites in aldol condensation of ketones. Especially, we systematically investigated the catalyst activity of 80 %$Hf_{1.5}$TPA/MCM-41 in aldol condensation of cyclopentanone and cyclohexanone and realized the co-aldol condensation of lignocellulosic ketones in one-pot reaction. By characterization, the good performance of the catalyst is attributed to the Hf doping, which changes the electronic structure of the catalyst surface and creates new strong L acid and improves the catalyst stability by anti-coking and water tolerance. This work suggests a simple way to synthesize high-performance aldol condensation acid catalyst and potentially promotes the industrialization process of bio-Jet fuel synthesis.

CRediT authorship contribution statement

Qi Li: Data curation, Formal analysis, Writing – original draft. **Genkuo Nie:** Conceptualization, Methodology, Supervision, Investigation, Writing – original draft, Project administration, Funding acquisition, Writing – review & editing. **Hongyu Wang:** Software, Formal analysis, Resources, Data curation. **Ji-Jun Zou:** Writing – review & editing. **Shitao Yu:** Writing – review & editing. **Hailong Yu:** Formal analysis. **Xin Jin:** Validation. **Dongpei Zhang:** Data curation. **Huibing Shi:** Investigation. **Deming Zhao:** Investigation.

Declaration of Competing Interest

The authors declare that they have no known competing financial interests or personal relationships that could have appeared to influence the work reported in this paper.

Data Availability

Data will be made available on request.

Acknowledgments

This work was supported by the National Natural Science Foundation of China (2210081015), the Talent Foundation funded by Province and Ministry Co-construction Collaborative Innovation Center of Eco-chemical Engineering (STHGYX2222), the Open Fund of the Key Laboratory of Multiphase Flow Reaction and Separation Engineering of Shandong Province (2021MFRSE-B01).

Appendix A. Supporting information

Supplementary data associated with this article can be found in the online version at doi:10.1016/j.apcatb.2022.122330.

References

[1] J.-J. Zou, G. Nie, Design and synthesis of high-density fuels from biomass. In High-Energy-Density Fuels for Advanced Propulsion, John Wiley & Sons, 2020, pp. 241–289.

[2] G. Nie, H. Wang, Q. Li, L. Pan, Y. Liu, Z. Song, X. Zhang, J.-J. Zou, S. Yu, Co-conversion of lignocellulosic derivatives to jet fuel blending by an efficient hydrophobic acid resin, Appl. Catal. B (2021), 120181.

[3] J. Sun, S. Shao, X. Hu, X. Li, H. Zhang, Synthesis of oxygen-containing precursors of aviation fuel via carbonylation of the aqueous bio-oil fraction followed by C–C coupling, ACS Sustain. Chem. Eng. 10 (2022) 11030–11040.

[4] L.T. Mika, E. Csefalvay, A. Nemeth, Catalytic conversion of carbohydrates to initial platform chemicals: chemistry and sustainability, Chem. Rev. 118 (2018) 505–613.

[5] B. Qiu, X. Tao, J. Wang, Y. Liu, S. Li, H. Chu, Research progress in the preparation of high-quality liquid fuels and chemicals by catalytic pyrolysis of biomass: a review, Energy Convers. Manag. 261 (2022), 115647.

[6] X. Sheng, G. Li, W. Wang, Y. Cong, X. Wang, G.W. Huber, N. Li, A. Wang, T. Zhang, Dual-bed catalyst system for the direct synthesis of high density aviation fuel with cyclopentanone from lignocellulose, AlChE J. 62 (2016) 2754–2761.

[7] J. Yang, N. Li, G. Li, W. Wang, A. Wang, X. Wang, Y. Cong, T. Zhang, Synthesis of renewable high-density fuels using cyclopentanone derived from lignocellulose, Chem. Commun. 50 (2014) 2572–2574.

[8] W. Wang, N. Li, G. Li, S. Li, W. Wang, A. Wang, Y. Cong, X. Wang, T. Zhang, Synthesis of renewable high-density fuel with cyclopentanone derived from hemicellulose, ACS Sustain. Chem. Eng. 5 (2017) 1812–1817.

[9] J. Xu, N. Li, X. Yang, G. Li, A. Wang, Y. Cong, X. Wang, T. Zhang, Synthesis of diesel and jet fuel range alkanes with furfural and angelica lactone, ACS Catal. 7 (2017) 5880–5886.

[10] J. Xie, L. Zhang, X. Zhang, P. Han, J. Xie, L. Pan, D.-R. Zou, S.-H. Liu, J.-J. Zou, Synthesis of high-density and low-freezing-point jet fuel using lignocellulose-derived isophorone and furanic aldehydes, Sustain. Energy Fuels 2 (2018) 1863–1869.

[11] Q. Deng, G. Nie, L. Pan, J.-J. Zou, X. Zhang, L. Wang, Highly selective self-condensation of cyclic ketones using MOF-encapsulating phosphotungstic acid for renewable high-density fuel, Green. Chem. 17 (2015) 4473–4481.

[12] Y. Jing, Y. Xin, Y. Guo, X. Liu, Y. Wang, Highly efficient Nb_2O_5 catalyst for aldol condensation of biomass-derived carbonyl molecules to fuel precursors, Chin. J. Catal. 40 (2019) 1168–1177.

[13] A.N. Migues, Q. Sun, S. Vaitheeswaran, W. Sherman, S.M. Auerbach, On the rational design of zeolite clusters for converging reaction barriers: Quantum study of aldol kinetics confined in HZSM-5, J. Phys. Chem. C. 122 (2018) 23230–23241.

[14] R. Wang, Y. Liu, G. Li, A. Wang, X. Wang, Y. Cong, T. Zhang, N. Li, Direct synthesis of methylcyclopentadiene with 2,5-hexanedione over zinc molybdates, ACS Catal. (2021) 4810–4820.

[15] Y. Qi, Z. Liu, S. Liu, L. Cui, Q. Dai, C. Bai, Production of a renewable functionalized 1,3-diene from furfural-acetone adduct over supported heteropolyacid catalysts, ACS Sustain. Chem. Eng. 8 (2020) 7214–7224.

[16] S.-S. Wang, G.-Y. Yang, Recent advances in polyoxometalate-catalyzed reactions, Chem. Rev. 115 (2015) 4893–4962.

[17] X. Lopez, J.J. Carbo, C. Bo, J.M. Poblet, Structure, properties and reactivity of polyoxometalates: a theoretical perspective, Chem. Soc. Rev. 41 (2012) 7537–7571.

[18] J. Zhong, J. Pérez-Ramírez, N. Yan, Biomass valorisation over polyoxometalate-based catalysts, Green. Chem. 23 (2021) 18–36.

[19] I.V. Kozhevnikov, Catalysis by heteropoly acids and multicomponent polyoxometalates in liquid-phase reactions, Chem. Rev. 98 (1998) 171–198.

[20] G. Nie, J.-J. Zou, R. Feng, X. Zhang, L. Wang, HPW/MCM-41 catalyzed isomerization and dimerization of pure pinene and crude turpentine, Catal. Today 234 (2014) 271–277.

[21] Y. Liu, G. Nie, S. Yu, L. Pan, L. Wang, X. Zhang, C. Shi, J.-J. Zou, Water-tolerant phosphotungstic acid catalyst for controllable synthesis of high-performance biojet fuel, Chem. Eng. Sci. 238 (2021), 116592.

[22] R. Balaga, P. Yan, K. Ramineni, H. Du, Z. Xia, M.R. Marri, Z.C. Zhang, The role and performance of isolated zirconia sites on mesoporous silica for aldol condensation of furfural with acetone, Appl. Catal. A-Gen. 648 (2022), 118901.

[23] O. Kikhtyanin, D. Kubička, J. Čejka, Toward understanding of the role of Lewis acidity in aldol condensation of acetone and furfural using MOF and zeolite catalysts, Catal. Today 243 (2015) 158–162.

[24] A. Popa, V. Sasca, I. Holclajtner-Antunović, The influence of surface coverage on textural, structural and catalytic properties of cesium salts of 12-molybdophosphoric acid supported on SBA-15 mesoporous silica, Micro Mesopor. Mat. 156 (2012) 127–137.

[25] W.-L. Peng, J. Mi, F. Liu, Y. Xiao, W. Chen, Z. Liu, X. Yi, W. Liu, A. Zheng, Accelerating biodiesel catalytic production by confined activation of methanol over high-concentration ionic liquid-grafted UiO-66 solid superacids, ACS Catal. 10 (2020) 11848–11856.

[26] Z. Wang, C. Wang, S. Mao, B. Lu, Y. Chen, X. Zhang, Z. Chen, Y. Wang, Decoupling the electronic and geometric effects of Pt catalysts in selective hydrogenation reaction, Nat. Commun. 13 (2022) 3561.

[27] M.J. Da Silva, A.A. Julio, S.O. Ferreira, R.C. Da Silva, D.M. Chaves, Tin(II) phosphotungstate heteropoly salt: An efficient solid catalyst to synthesize bioadditives ethers from glycerol, Fuel 254 (2019), 115607.

[28] M.J. da Silva, D.M. Chaves, S.O. ferreira, R.C. da Silva, J.B. Gabriel Filho, C.G. O. Bruziquesi, A.A. Al-Rabiah, Impacts of Sn(II) doping on the Keggin heteropolyacid-catalyzed etherification of glycerol with tert-butyl alcohol, Chem. Eng. Sci. 247 (2022), 116913.

[29] H.M.A. Hassan, M.A. Betiha, A.E.R.S. Khder, M. Mostafa, M. Gallab,Hassan, Hafnium pentachloride ionic liquid for isomorphic and postsynthesis of HfKIT-6 mesoporous silica: catalytic performances of Pd/SO_4^{2-}/HfKIT-6, J. Porous Mater. 23 (2016) 1339–1351.

[30] I.B. Polovov, Y.S. Bataev, Y.D. Afonin, V.A. Volkovich, A.V. Chukin, A. Rakhmatullin, M. Boča, Synthesis of HfO_2, Hafnium Hydroxide Hydrate, J. Alloy. Compd. 790 (2019) 405–412.

[31] M.N. Sokolov, E.V. Chubarova, E.V. Peresypkina, A.V. Virovets, V.P. Fedin, Complexes of ZrIV and HfIV with monolacunary Keggin-and Dawson-type anions, Russ. Chem. Bull. 56 (2007) 220–224.

[32] T. Kidchob, L. Malfatti, F. Serra, P. Falcaro, S. Enzo, P. Innocenzi, Hafnia sol-gel films synthesized from $HfCl_4$: changes, Struct. Prop. firing Temp., J. Sol. -Gel Sci. Technol. 42 (2007) 89–93.

[33] W. Liao, L. Qi, Y. Wang, J. Qin, G. Liu, S. Liang, H. He, L. Jiang, Interfacial engineering promoting electrosynthesis of ammonia over Mo/Phosphotungstic acid with high performance, Adv. Funct. Mater. 31 (2021) 2009151.

[34] W. Liao, H.-X. Liu, L. Qi, S. Liang, Y. Luo, F. Liu, X. Wang, C.-R. Chang, J. Zhang, L. Jiang, Lithium/bismuth co-functionalized phosphotungstic acid catalyst for promoting dinitrogen electroreduction with high faradaic efficiency, Cell Rep. Phys. Sci. 2 (2021), 100557.

[35] Y. Chen, X. Yao, X. Wang, X. Zhang, H. Zhou, R. He, Q. Liu, Direct use of the solid waste from oxytetracycline fermentation broth to construct Hf-containing catalysts for Meerwein-Ponndorf-Verley reactions, RSC Adv. 11 (2021) 13970–13979.

[36] X. Yi, H.-H. Ko, F. Deng, S.-B. Liu, A. Zheng, Solid-state ^{31}P NMR mapping of active centers and relevant spatial correlations in solid acid catalysts, Nat. Protoc. 15 (2020) 3527–3555.

[37] S. Xin, Q. Wang, J. Xu, Y. Chu, P. Wang, N. Feng, G. Qi, J. Trébosc, O. Lafon, W. Fan, F. Deng, The acidic nature of “NMR-invisible” tri-coordinated framework aluminum species in zeolites, Chem. Sci. 10 (2019) 10159–10169.

[38] I. Ro, J. Qi, S. Lee, M. Xu, X. Yan, Z. Xie, G. Zakem, A. Morales, J.G. Chen, X. Pan, D.G. Vlachos, S. Caratzoulas, P. Christopher, Bifunctional hydroformylation on heterogeneous Rh-WOx pair site catalysts, Nature 609 (2022) 287–292.

[39] D. Fang, J. Yang, C. Jiao, Dicationic ionic liquids as environmentally benign catalysts for biodiesel synthesis, ACS Catal. 1 (2011) 42–47.

[40] M. Wan, D. Liang, L. Wang, X. Zhang, D. Yang, G. Li, Cycloketone condensation catalyzed by zirconia: origin of reactant selectivity, J. Catal. 361 (2018) 186–192.

[41] J. Yang, S. Li, N. Li, W. Wang, A. Wang, T. Zhang, Y. Cong, X. Wang, G.W. Huber, Synthesis of jet-fuel range cycloalkanes from the mixtures of cyclopentanone and butanal, Ind. Eng. Chem. Res. 54 (2015) 11825–11837.

[42] W. Wang, X. Ji, H. Ge, Z. Li, G. Tian, X. Shao, Q. Zhang, Synthesis of C_{15} and C_{10} fuel precursors with cyclopentanone and furfural derived from hemicellulose, RSC Adv. 7 (2017) 16901–16907.